Solvent-Free Mechanochemical Approach towards Thiospinel MgCr2S4 as a Potential Electrode for Post-Lithium Ion Batteries

batteries

MDPI

Article

Solvent-Free Mechanochemical Approach towards Thiospinel $MgCr_2S_4$ as a Potential Electrode for Post-Lithium Ion Batteries

Laura Caggiu [1,*], Stefano Enzo [1], Lorenzo Stievano [2,3], Romain Berthelot [2], Claudio Gerbaldi [4], Marisa Falco [4], Sebastiano Garroni [1] and Gabriele Mulas [1,*]

1 Department of Chemistry and Pharmacy, University of Sassari and INSTM, Via Vienna 2, I-07100 Sassari, Italy; enzo@uniss.it (S.E.); s.garroni@uniss.it (S.G.)
2 ICG-AIME, Bat 15, University of Montpellier 2, Pl. E. Bataillon, 34095 Montpellier CEDEX, France; lorenzo.stievano@umontpellier.fr (L.S.); romain.berthelot@umontpellier.fr (R.B.)
3 Réseau sur le Stockage Electrochimique de l'Energie (RS2E), CNRS FR3459, 33 Rue Saint Leu, 80039 Amiens CEDEX, France
4 GAME Lab, Department of Applied Science and Technology—DISAT, Politecnico di Torino, Corso Duca Degli Abruzzi 24, 10129 Torino, Italy; claudio.gerbaldi@polito.it (C.G.); marisa.falco@polito.it (M.F.)
* Correspondence: lcaggiu@uniss.it (L.C.); mulas@uniss.it (G.M.)

Received: 20 July 2020; Accepted: 19 August 2020; Published: 24 August 2020

Abstract: Several new compounds, with desirable properties of ion mobility and working voltage, have been recently proposed using a density functional theory (DFT) computational approach as potential electrode materials for beyond-lithium battery systems. After evaluation of the 'energy above hull', thiospinel $MgCr_2S_4$ has been suggested as interesting multivalent battery cathode candidate, even though the synthesis of its exact stoichiometry poses serious challenges. In this work, $MgCr_2S_4$ is prepared using an innovative mechanochemical route starting from magnesium or magnesium hydride, chromium, and sulfur powders. The progress of such mechanically induced reaction as a function of processing time is carefully monitored by XRD with Rietveld refinement, evidencing the occurrence of a mechanically induced self-propagating reaction (MSR). The effect of parameters associated with the milling apparatus (impact energy) on the products composition are also investigated. To our knowledge, this work represents the first report of the scalable and simple mechanical alloying synthesis of thiospinel $MgCr_2S_4$ (space group Fd-3 m, a = 10.09 Å) and opens up interesting possibilities for the exploitation of such material in next-generation post-lithium batteries.

Keywords: thiospinel; $MgCr_2S_4$; self-sustaining reaction; mechanochemistry; post-lithium battery; multivalent battery cathode

1. Introduction

In the framework of the increasingly high demand for electrical energy storage (EES) systems [1,2], smart grid, and stationary power networks, particular attention is focused on secondary batteries. For this reason, materials viable for these applications are the epicenter of many studies, including new computational compounds with theoretically suitable electrochemical characteristics [3]. Among the secondary batteries, Li-based chemistries display the highest practical gravimetric energy density, and besides the widespread use in electronic devices, they are more and more employed in hybrid-electric and full-electric vehicles [4,5]. In 2016, LIB market reached over US $20 billion, US $5 billion of which specifically for the automotive industry [6]. This growing market will drive the increase of lithium demand, and most likely its price, since lithium is becoming a critical element, due to its limited availability and often problematic supply chain [7].

For these reasons, researchers worldwide have directed their attention towards alternative elements able, in the form of ions, to intercalate into specific hosts in a reversible manner via the so-called rocking chair mechanism, thus allowing the processes of charge and discharge. The most available elements suitable for this purpose are Mg, Zn, Ca, Al, and Na [8,9]. Among these, Mg [10–15] emerges due to its high abundance on the Earth's crust (~13%) and high volumetric capacity (3832 mAh cm^{-3}) [16].

Considering the promising electrochemical activity of the compounds with a spinel structure as cathodes for LIBs [17], this class of materials has also been tested in magnesium batteries [18–20]. However, the slow kinetics of magnesium in spinels prompted research on the sister thiospinel compounds, where the replacement of oxide with sulfide ions enables a softer interaction with Mg^{2+} and thus more favorable diffusion barriers [21]. These properties were confirmed in a theoretical DFT (density functional theory) study by Liu et al. [22], who investigated the properties of a group of first row transition-metal thiospinels and showed that the compound with the lowest energy above hull—i.e., the product more thermodynamically stable with respect to the reagents and therefore easier to synthesize—is the host Cr_2S_4.

Given the potential mobility of Mg^{2+} in the Cr_2S_4 host, the synthesis of thiospinel $MgCr_2S_4$ has attracted many attentions in the last period, as emerged from the recent literature [23,24]. For example, Poeppelmeier et al. [23] have obtained the Mg-based thiospinel by thermal annealing at 800 °C under vacuum for 2 weeks, followed by a further treatment with H_2SO_4 acid to recover the ternary phase. The pure compound was synthesized by Ceder et al. [24] by a metathesis reaction between $NaCrS_2$ and $MgCl_2$, which involved two different steps: a ball milling treatment of 14 h and a thermal annealing at 500 °C. However, despite these achievements, the prolonged treatments and the use of hazardous solvents can significantly limit the extensive use of the aforementioned chemical approaches. An alternative way can be offered by mechanochemistry, which is largely exploited for the solvent-free production of nanostructured functional materials. It can represent a valid technique that may overcome the barrier of immiscibility between chromium and magnesium [25,26]. In addition, compared to common thermal synthesis methods, mechanical processing through high-energy ball milling (BM) is simple, energetically convenient, and easily upscalable at the industrial level. To the best of our knowledge, the mechanochemical preparation of $MgCr_2S_4$ has not yet been explored. In this work, the preparation of the ternary thiospinel was attempted by mechanical treatment trough high energy BM. The transformation occurred during the mechanochemical reaction was studied by X-ray powders diffraction and scanning electron microscopy.

2. Results and Discussion

The mechanochemical synthesis of the thiospinel $MgCr_2S_4$ has been approached by using a SPEX Mixer/Mill 8000 apparatus equipped with a stainless-steel vial adapted for monitoring the reaction temperature. More information about the experimental setup are provided in Section 3.

The use of magnesium hydride instead of magnesium was experimented because of the higher reactivity of the former and for its capability to react with S and Cr under mechanochemical stimulation. For example, Goo and Hirscher [27] obtained MgS by high energy ball milling, starting from MgH_2 and S. In other works, the use of MgH_2 with Cr resulted in a ternary Mg-H-Cr phase [28].

For the first test with MgH_2, exploratory experiments were performed using appropriate quantities of MgH_2, Cr, and S, following the stoichiometry of the desired thiospinel as reported in Equation (1)

$$MgH_2 + 4S + 2Cr \rightarrow MgCr_2S_4 + H_2\uparrow \quad (1)$$

Figure 1 shows a series of XRD patterns collected from mixtures of the processed reagents (MgH_2, Cr, and S) as a function of the milling times. The starting reagents (bottom pattern, 0.5 h/1800 s) were tetragonal MgH_2, space group (SG) P42/mnm, cubic Cr, space group Im-3 m and orthorhombic S, space group Fddd:2, and their estimated relative weights in percentage were 10.8, 38.3, and 50.9 wt%, respectively. The Rietveld analysis of the pattern acquired for the specimen milled for 1 h (3600 s)

evidenced that the average crystallite size of MgH_2 was decreased to ca. 960 Å, while those of Cr and S changed slightly (see Table S1 for details). This trend was confirmed for increasing milling times: in the systems milled for 2 h (7200 s) and 4 h (14,400 s), only the initial reagents were present. The average crystallite size of MgH_2 further decreased up to 420 Å, while a modest variation was observed in those of Cr and S (420 and 1180 Å, respectively). In addition, the lattice parameters of the three systems did not vary significantly as a function of milling times, thus making it possible to exclude the formation of solid solutions between the reagents.

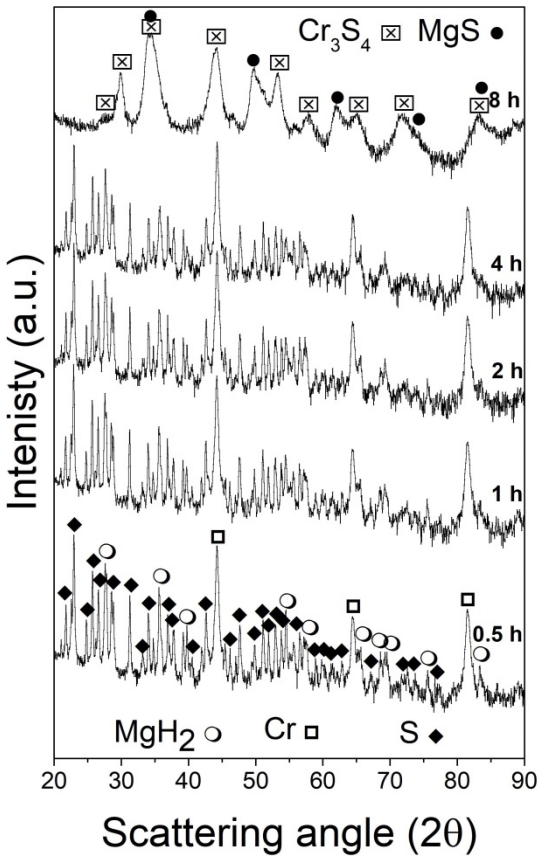

Figure 1. XRD powder patterns of the MgH_2 + 2Cr + 4S system mixture subjected to the mechanical treatment for increasing periods of times indicated (from 0.5 to 8 h from bottom to top).

After 8 h (28,800 s), the presence of MgS and Cr_3S_4 (Brezianite) was identified thanks to their intense reflections (34.56°, 49.68° for MgS; and 30.02°, 33.96°, 44.07°, and 53.23° for Cr_3S_4), as shown in the top pattern in Figure 1, while the Bragg reflections associated with the starting reagents completely disappeared. A third unknown phase seems to emerge from the analyzed pattern.

During the synthesis, the external temperature of the mechanochemical reactor increased significantly. This, in combination with the instantaneous conversion of reagents, is often an indication of a mechanically induced self-sustaining reaction (MSR) process [29], as sometimes observed when metal chalcogenides are synthesized from their corresponding elements [30]. To verify this aspect, the temperature of the reaction vial was monitored over time, under the same specific mechanochemical conditions. The recorded temperature profile is shown in Figure 2, and it consists of three main steps, as usually observed for a mechanically-induced MSR process. In the first step, known as induction or activation period, the particles and/or crystallites are subjected to size reduction reaching a critical limit after 290 min (17,400 s). This was proven by XRD, in particular for MgH_2. The temperature increase observed during this step (+10 °C), was principally due to the heat dissipation through the walls of the vial. The second step, corresponding to an abrupt increase of the temperature up to 49 °C (ΔT = 23 °C in few seconds), is referred to as the ignition time and it is the consequence of the combustion front

propagating through the powders charged. In the final step, the temperature decreases rapidly to a value similar to that before the ignition event. During this step, the evolution of the product structure takes place. In order to further investigate this reaction, the solid obtained just after the ignition time, after 5 h (18,000 s) of BM, was inspected by scanning electron microscopy (Figure 3) and XRD (Figure 4).

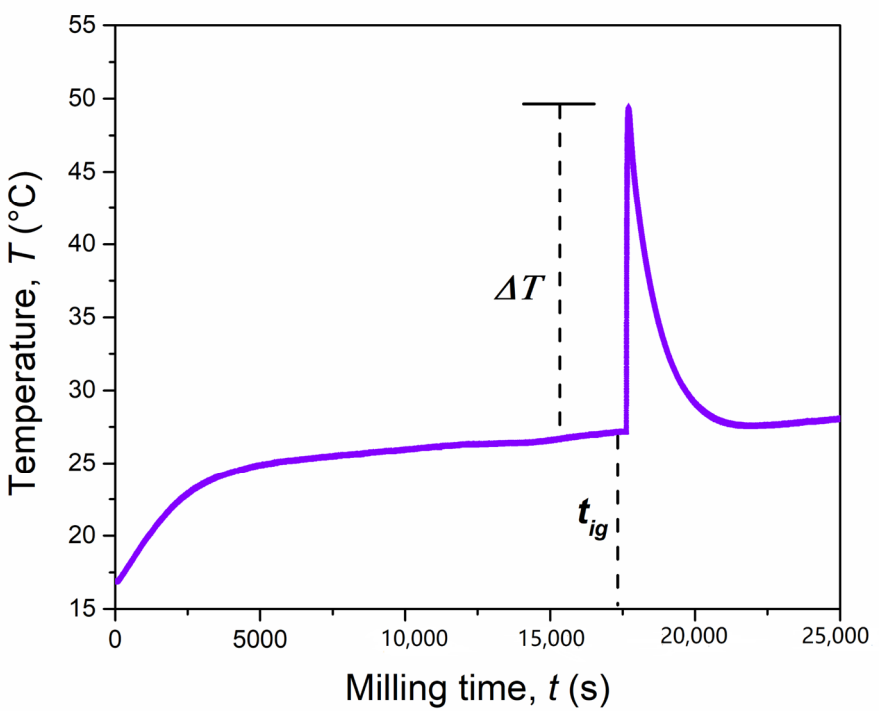

Figure 2. Temperature profile of the mechanochemical reactor during the reaction of the MgH_2 + 2Cr + 4S system (4 g) milled at 875 rpm by using a single ball of 8 g.

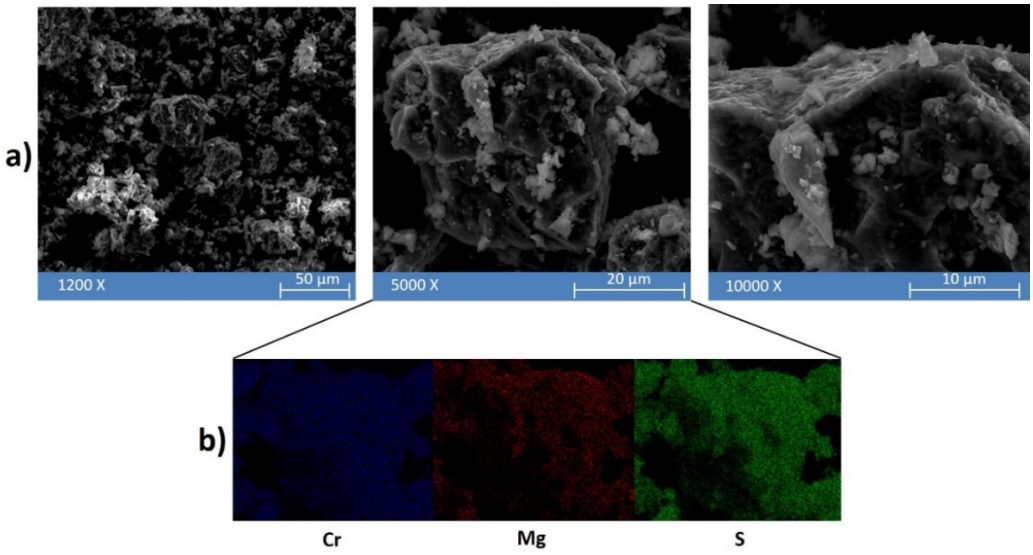

Figure 3. (**a**) Representative SEM micrographs at different magnifications of the MgH_2 + 2Cr + 4S powders after 5 h of high energy ball milling. (**b**) Energy dispersive spectroscopy (EDS) analysis applied to an agglomerate (middle panel) observed in the powder mixture.

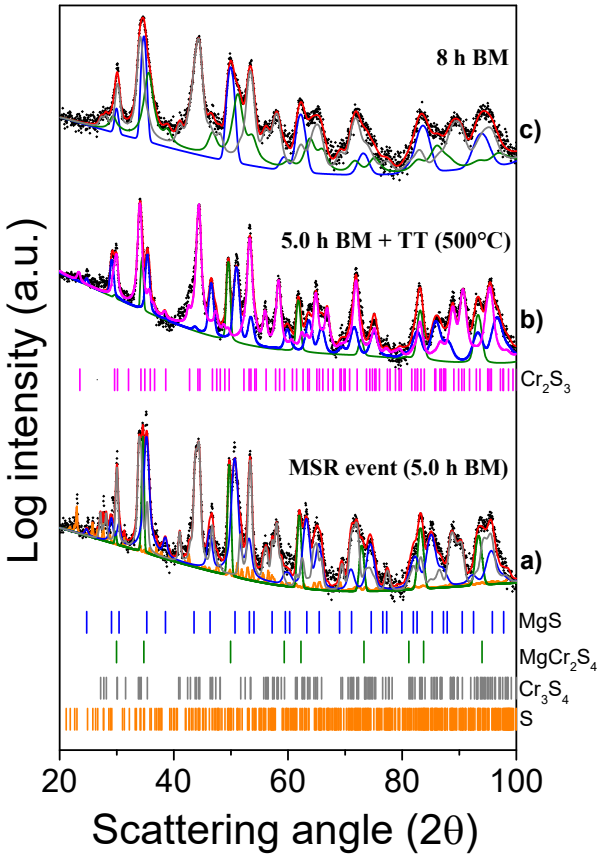

Figure 4. XRD patterns of the MgH_2 + 2Cr + 4S system milled for 5 h (**a**), post-annealed at 500 °C (**b**), and then again milled for 8 h (**c**).

At low magnification (12,000 X—Figure 3a left panel) it is possible to observe that the plastic deformation and agglomeration of the particles are predominant. The powders were actually characterized by agglomerates of around 40–60 μm, as usually observed after MSR [31]. Furthermore, the presence of irregular cavities observed at high magnification (5000 X—Figure 3a central panel) can be ascribed to self-propagating high-temperature reactions. The elemental composition of a representative agglomerate was characterized by EDS (Figure 3b): three main elements were detected—viz. Mg, Cr, and S—which were homogenously distributed on the agglomerate, suggesting a quite uniform composition of the solid mixture formed upon ignition. However, a higher concentration of Mg is localized in the small particles of 2–0.5 μm detected on the surface of the agglomerates, as shown in the right panel of Figure 3.

The XRD pattern of the system milled for 5 h (18,000 s) shows a variety of peaks attributed to MgS and Cr_3S_4 (Figure 4a), also detected in the system milled for 8 h (28,800 s). Moreover, some additional peaks (29.25°, 35.21°, 46.55°, and 50.66°) show a progression typical of cubic spinels. The powders collected at the ignition time were then analyzed by DSC from 20 to 500 °C. As evidenced in the thermogram (Figure S1), no obvious reaction occurs in the investigated temperature range. To confirm the absence of any thermally induced change in the composition of the mixture, the powder collected after the DSC analysis was further analyzed by XRD (Figure 4b). The first pattern (a) reported in Figure 4 was recorded right after the temperature increase caused by the MSR and it shows the presence of a new phase, differently from what observed after 4 h (14,400 s) in Figure 1—i.e., before the MSR—as discussed above.

Given that no crystal structure data are available for $MgCr_2S_4$, the CIF file of $CuCr_2S_4$ (COD ID 9012141, space group Fd-3 m) was used to refine the experimental pattern and prove the formation of the Mg-based thiospinel. In this case, the absorption coefficient of Cu was replaced with that of

Mg, and the cell parameter a was refined to 10.09 Å. The asymmetric unit in spinels is made by Mg at (0, 0, 0) with a multiplicity of 8; Cr at (0.625, 0.625, 0.625) with a multiplicity of 16 and S at (0.385, 0.385, 0.385) with a multiplicity of 32 [32]. Poeppelmeier et al. [25] also reported the formation of $MgCr_2S_4$ with the same space group and a very similar cell parameter of 10.143 Å. Typically, in an AB_2S_4 spinel, the A and B cations occupy the tetrahedral and octahedral positions, respectively. In the case of inverse spinels, half of the B cations occupy the tetrahedral positions, and the octahedral sites are occupied by the A and the remaining B cations [33]. Changing the positions occupancy, the coordination number of an element and its ionic radius may vary consequently ($Mg^{2+}_{(4)}$ = 49 pm, $Mg^{2+}_{(6)}$ = 72 pm, $Cu^{2+}_{(4)}$ = 57 pm, $Cu^{2+}_{(6)}$ = 73 pm) [33]. This fact might explain the expansion of the cell going from $CuCr_2S_4$ to the $MgCr_2S_4$ phase obtained in this study (9.800 Å for $CuCr_2S_4$ and 10.09 Å for $MgCr_2S_4$, respectively).

Based on the Rietveld refinement, the formed ternary thiospinel phase, at the MSR event, amounts to 30 wt%, while the MgS and Cr_3S_4 phases were 30 and 36 wt%, respectively. Furthermore, traces of S (4.0 wt%) were also detected. The analysis of both the patterns collected after 5 h (18,000 s) of BM in Figure 4a,b confirmed that the composition of the powder is similar before and after the thermal treatment: Cr_3S_4 is transformed into Cr_3S_2 consuming the residual sulfur, while MgS and $MgCr_2S_4$ can still be detected in the annealed powders.

Finally, the XRD pattern of the system milled for 8 h (28,800 s) (Figure 4c), was properly interpolated with MgS (33 wt%), Cr_3S_4 (52 wt%) and the thiospinel $MgCr_2S_4$ (15 wt%) phases. It is also important to highlight that all peaks broadened and decreased in intensity, while an increase of the whole pattern background was observed. A significant reduction of the crystallite size was estimated for all the phases (MgS = 811 Å, Cr_3S_4 = 513 Å, and $MgCr_2S_4$ = 80 Å). This indicates that for longer milling times, the thiospinel phase can gradually turn into a mixture of nanocrystalline and amorphous phases, and, for this reason, its relative amount might be underestimated. However, even though $MgCr_2S_4$ is supposed to be one of the thermodynamically favored products (Table 1), the possibility that it decomposes into other Mg- and Cr- sulfides during prolonged BM cannot be disregarded.

Table 1. Reagents used for synthesis, the compounds obtained from it and their enthalpies of formation of the MgH_2 + 2Cr + 4S system. Comparing these latter values, the desired ternary phase emerges as the most thermodynamically favored product.

Reagents	$\Delta_f H^\circ$ (KJ mol^{-1} at 298 K)	Products	$\Delta_f H^\circ$ (KJ mol^{-1} at 298 K)
MgH_2	−75.30 [34]	Cr_2S_3, Cr_3S_4	−467.14 and −629.67 [35]
Cr	0.00 [34]	MgS	−346.00 [34]
S	0.00 [34]	$MgCr_2S_4$	−869.90 [36]

Remarkably, the yield (30 wt%) of thiospinel reported in this work after 5 h (18,000 s) of BM, was slightly higher than that achieved by Poeppelmeier and coauthors [25]. In the first step they obtained a similar mixture of phases, but in their case, a thermal treatment of the starting reagents (Mg, Cr, and S) for 168 h (1 week) at 800 °C was necessary. Moreover, they evidenced that further annealing at 1000 °C promoted the decomposition of thiospinel to Cr and Mg-based sulfides.

Despite the evident benefits here demonstrated, the self-sustaining reaction induced by mechanical processing presents a limitation when MgH_2 is used as magnesium source: at around 5 h BM, the evolution of H_2S (colorless and toxic gas) was detected by a lead acetate paper strip attached at the bottom of the vial during the experiment (see Figure S2a). At the MSR event, the paper strip turned to black because of lead sulfide formation (Figure S2b), showing that this synthesis approach is not suitable for the preparation of thiospinels, since sulfur is removed from the solid-state reaction. Therefore, the synthesis was also attempted using Mg instead of magnesium hydride under the same mechanochemical conditions, in terms of amount of powders, ball mass, stoichiometric molar ratio between reagents, as well as milling speed.

The XRD patterns of the reactants mixture ball milled for 1 h (3600 s), 2 h (7200 s), and 4 h (14,400 s) are compared in Figure 5a–c with those of the system processed for increasing milling times at 6 h

20 min (22,800 s), 8 h (28,800 s), and 16 h (57,600 s) (Figure 5d–f). The results of the Rietveld analysis (cf. Table S2) for short milling times simply show the presence of a mixture of the starting reagents (Cr = 36.6 wt%, Mg = 14.1 wt% and S = 49.3 wt%). As for the MgH_2-based system, the crystallite sizes of Cr and S did not change significantly during the initials hours of milling, while those related to the Mg powders decreased from 1630 to 726 Å (4 h/7200 s BM). At this value of milling time, the milling temperature was stable at 28 °C, as indicated in Figure 6. After around 6 h 20 min (22,800 s) of BM, indicated in the picture as t_{ig}, the temperature promptly increased from 28 °C to 49 °C (ΔT = 21 °C). The effect produced by the MSR reaction can be deduced from the related XRD patterns shown in Figure 5d. The presence of the $MgCr_2S_4$ peaks is evident, along with those corresponding to the Cr_3S_4, MgS, and S (residual) phases.

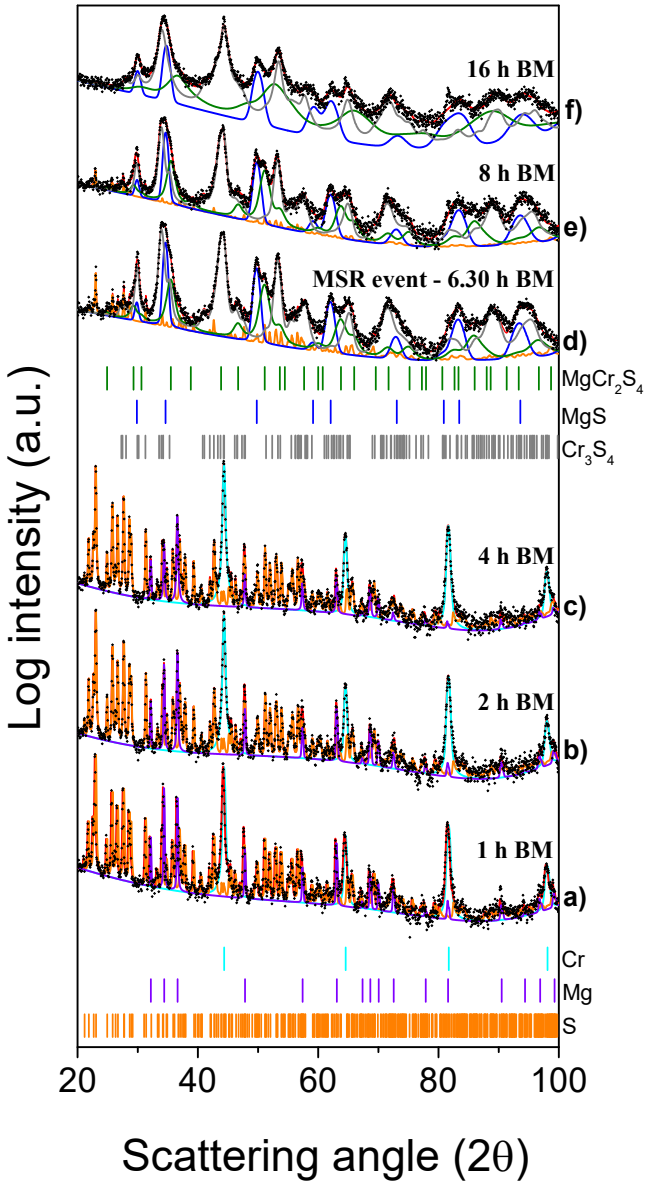

Figure 5. XRD patterns of the Mg + 2Cr + 4S system mixture subjected to the mechanical treatment for the times indicated (1 to 16 h from (**a**–**f**).

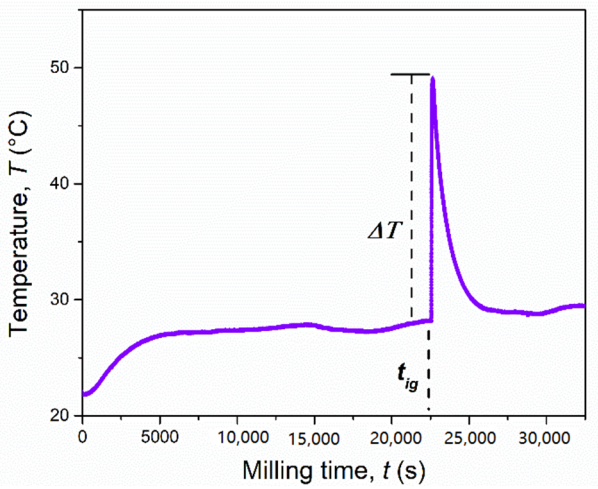

Figure 6. Temperature profile of the mechanochemical reactor during the reaction of the Mg + 2Cr + 4S system (4 g) milled at 875 rpm by using a single ball of 8 g.

As estimated by the Rietveld analysis (Table S2), the thiospinel content was 13 wt% and the corresponding crystallite size was approximately 137 Å. Longer milling times correspond to the reduction of the crystallite sizes of the three phases: after 8 h (28,800 s) of BM (Figure 5e), the average crystallite sizes were 101, 182, and 750 Å for the $MgCr_2S_4$, Cr_3S_4, and MgS phases, respectively. With respect to the previous experiment, prolonging the milling time to 16 h produces a further reduction of the crystallite size of the thiospinel (32 Å) together with a partial amorphization of the system, as emerged from the significant increase of the pattern background shown in Figure 5f.

Concerning the difference between the two processes, it was possible to highlight that the MSR event occurred for both the MgH_2- and Mg-based reactions, but with two main differences: if on one hand the evolution of H_2S was definitely suppressed by replacing magnesium hydride with magnesium metal, on the other hand, the ignition time was significantly longer in the latter case (5 h vs. 6 h, 20 min). This could be ascribed to the fact that the metal hydride is more brittle and less ductile than the metal, thus allowing a more efficient milling process.

The occurrence of a mechanically induced self-propagating reaction and the ignition time at which it takes place depends on several factors strictly related to the energy transfer at impact E [37]. In particular, in order to optimize the MSR process, it may be of interest to determine an impact energy threshold, E_0, above which the combustive reaction occurs. To get this parameter, further new experiments on the Mg + 2Cr+ 4S system were conducted at different impact energy E, by varying the milling speed, as indicated in Table 2. The recorded temperature profiles, as well as the corresponding XRD patterns acquired upon the combustive reaction, are available in the supporting information section (see Figures S3 and S4, respectively).

Table 2. Milling parameters for the Mg + 2Cr + 4S system milled at different impact energy

Powder Mass, m_p (g)	Ball Mass, m_b (g)	Milling Speed, ν (rpm)	Collision Frequency, N (Hz)	Impact Energy, E (J)	Ignition Time, t_{ig} (h)	Specific Energy Dose, D_{ig} (kJ g^{-1})
4	8	640	21.34	0.038	20.50	14.96
4	8	750	25.00	0.052	11.40	13.34
4	8	875	29.20	0.071	6.29	11.74
4	8	975	32.50	0.086	4.32	11.12
4	8	1000	33.30	0.090	4.01	11.029
4	2	875	29.20	0.017	NO MSR	-
4	8	555	18.50	0.014	NO MSR	-

By increasing the milling speed, which corresponds to a higher energy transferred to the powders through the impact, the ignition of the combustive reaction took place at shorter milling times, in agreement with previous works on MSR reactions [37]: with regard to such combustive mechanochemical reaction, a linear trend emerges when the reciprocal of the total number of collisions required for ignition $1/n_{ig}$, is plotted as a function of E (Figure 7a). The intercept extrapolated from the best-fitted line is E_0 = 0.018 J, which corresponds to the minimum impact energy necessary to activate the ignition process.

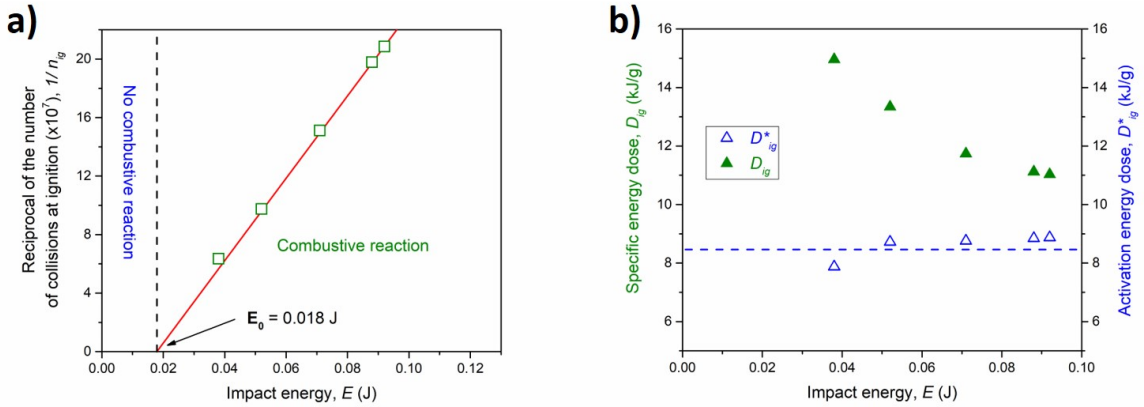

Figure 7. (**a**) The reciprocal number of collisions at ignition time as a function of the impact energy (green empty squares). The best linear fit is reported as a red line. (**b**) The specific energy dose (green full triangles) and the activation energy dose (blue empty triangles) as a function of the impact energy.

This result was experimentally confirmed by milling the starting reagents for more than 20 h (72,000 s) at impact energy per collision of 0.017 and 0.014 J (see Table 2). Considering the temperature profiles (Figure S5) recorded for both experiments, no MSR events were evidenced during the milling. Additionally, the X-ray diffraction patterns acquired at the end of the tests (Figure S6) were characterized by the presence of the starting reagents, with no formation of products. Interestingly, the average crystallite dimensions estimated for Mg were in the order of 350–400 Å, significantly smaller than those observed for the systems milled above the energy impact threshold E_0. This confirms that although a critical crystallite size must be reached to ignite the MSR, the process is mainly governed by the energy provided at each impact on the powders.

An additional step can be represented by the quantification of the mechanical work per unit of mass necessary to trigger the mechanochemical transformation. This parameter, also known as the specific energy dose D_{ig}, is related to the ignition time by the following Equation (2) [38]

$$D_{ig} = I_m \, t_{ig} \tag{2}$$

where I_m is the specific intensity of the mechanical treatment, which is linked to the energy E transferred to the powders through the impact by Equation (3)

$$I_m = \frac{NE}{m_p} \tag{3}$$

where N is referred to the frequency of collision and m_p is the mass of powders charged into the mechanochemical reactor. At the same time, an activation energy dose D_{ig}* can be defined, by combining Equations (2) and (3) with the quantity $E - E_0$, as reported in the equation

$$D_{ig}* = \frac{N(E - E_0)t_{ig}}{m_p} \tag{4}$$

According to Equations (2)–(4), the specific energy dose and the activation (or scaled) energy dose, were calculated and plotted as a function of the impacts energy in Figure 7b. The former, as expected, decreased for higher impact energy values, while the latter was nearly constant ($<D_{ig}^{*}>$ 8.42 kJ g^{-1}) for the whole interval of the energy supplied. These trends are in good agreement with previous investigations on MSR reactions in binary systems (such as Ti-C and Ti-S [38,39]) and confirm that activation energy dose is not influenced by the impact energy when an ignition energy threshold is considered. These mechanochemical quantities can be opportunely used to compare absolute base processes induced by mechanical and conventional thermal treatments, and they can be exploited for a better understanding of the mechanism.

3. Materials and Methods

To synthesize the desired ternary phase by BM, several tests were carried out varying the magnesium source (MgH_2 or Mg) and the milling time. The starting materials were: MgH_2 (Sigma-Aldrich 90.0%), Mg (Ventron 99.9%), Cr (Aldrich 99.5%), and S (Alpha Aesar 99.5%). The materials were handled under a protective argon atmosphere by using a Glove box (MBraun 20G), and for each experiment, the powders were sealed in a stainless-steel reactor with a single stainless steel ball. The mixtures were subjected to the mechanical process for increasing milling times, using a SPEX Mixer/Mill 8000 modified to operate at different rotation speeds (500–1200 rpm). The milling vial was equipped with a platinum sensor mounted on the outer surface, to monitor the temperature as a function of the reaction time, to assess the possible presence of mechanically induced self-propagating reactions (MSR) and to identify their ignition time. A representation of the experimental setup is shown in Figure 8.

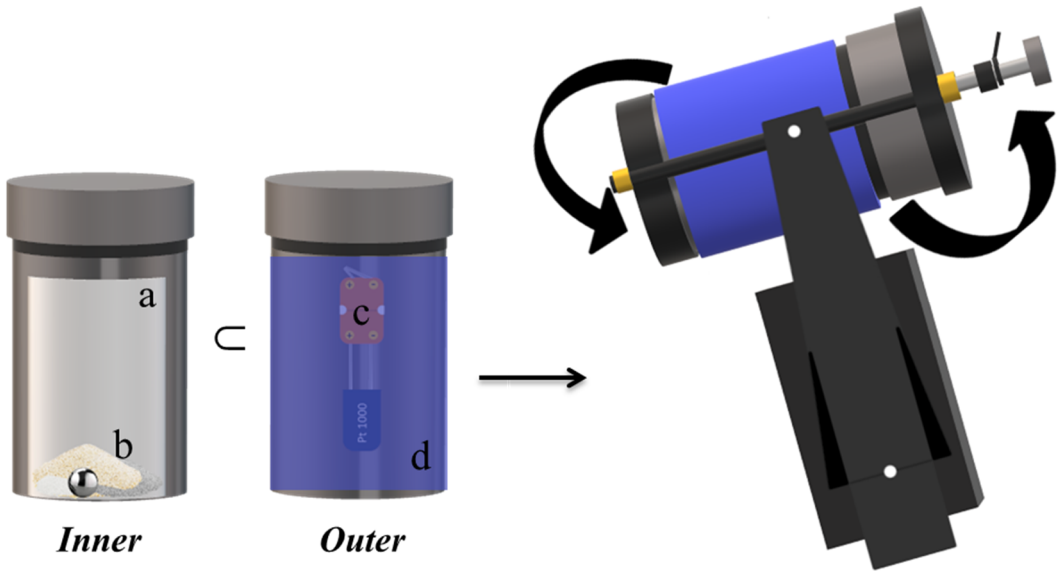

Figure 8. Schematic representation of the synthesis apparatus connected with a platinum sensor to monitor the vial temperature. (**a**) Vial, (**b**) powders and ball, (**c**) platinum sensor, (**d**) insulating jacket.

The X-ray powder diffraction (XRD) analysis was employed to gain information on the reaction products structure and to understand the kinetic evolution of the synthesis. To ensure the maintenance of an inert atmosphere during the XRD data collection, the samples were placed in an air-tight sample holder, sealed with a thin Kapton foil under argon atmosphere. The XRD analyses were carried out using a Bragg–Brentano rotating anode diffractometer (Smartlab Rigaku) equipped with a copper source ($Cu_{K\alpha 1}$ = 1.5406 Å, $Cu_{K\alpha 2}$ = 1.5443 Å). The patterns were collected step-wise in a 2θ range from 20° into 100°, with a step size of 0.05 and with a fixed time of 4 s. The XRD patterns were numerically refined by the Rietveld technique using the MAUD software [40].

The thermal analysis was carried out with a Setaram Labsys TG/DSC under Argon flux at a scanning rate equal to 10 °C min^{-1}, during a heating scan from 20 to 500 °C.

The morphological and elemental analyses of the powders were carried out by scanning electron microscopy (FEI Quanta 200).

4. Conclusions

$MgCr_2S_4$ (space group Fd-3 m, a = 10.09 Å) was successfully synthesized by mechanically induced self-sustaining reaction (MSR) starting from Cr, S, and Mg or MgH_2 reactants. In both cases, the mechanical processing was characterized by a rapid increase of the vial temperature, which is a clear evidence of the ignition step in the MSR reactions. For the system MgH_2:2Cr:4S, the MSR was induced after 5 h (18,000 s) of ball milling, with the formation of the solid phases $MgCr_2S_4$ (30 wt%), MgS, CrS, and the evolution of H_2S gas. Using Mg in the place of MgH_2, the generation of H_2S was suppressed and the formation of the thiospinel (13 wt%) occurred after 6 h 20 min of ball milling. Interestingly, the ternary cubic phase obtained with Mg reached the nanostructured condition (<50 Å) for prolonged ball milling times (>16 h) without decomposing to other side products nor singular elements. The experiments conducted at different impact energy enables estimation of the minimum impact energy (E_0 = 0.018 J) required to activate the ignition process of the combustive reaction and the minimum mechanical work transferred to the powders for triggering the mechanochemical transformation.

Overall, the mechanochemical synthesis was able to overcome the issues of immiscibility between the reagents, and allowed to obtain a substantial amount of $MgCr_2S_4$ using a lower quantity of energy as compared to the thermal synthesis, thus offering promising prospects for its possible up scalability at the industrial level.

Supplementary Materials: The following are available online at http://www.mdpi.com/2313-0105/6/3/43/s1, Table S1: Crystallographic parameters obtained by the Rietveld analysis for the system MgH_2 + 2Cr + 4S after mechanical treatment (with 8 g ball and 875 rpm); Table S2: Crystallographic parameters obtained from the Rietveld analysis for the system Mg + 2Cr + 4S after mechanical treatment (with 8 g ball and 875 rpm); Figure S1: DSC profile of the system MgH_2 + 2Cr + 4S collected at the ignition time of 5 h BM; Figure S2: Pictures captured before (2a) and after (2b) the MRS reaction. The white lead acetate paper (2a) becomes dark (b) upon BM for 5 h proving the H_2S evolution; Figure S3: Temperature profiles acquired during the experiments carried out at different milling speed of 640 (a), 750 (b), 975 (c) and 1000 (d) rpm; Figure S4: XRD patterns of the powders milled at different rotation speed and collected after the combustive reaction; Figure S5: Temperature profiles acquired during the experiments carried out varying the operative condition: 550 rpm with 8 g ball (E = 0.014 J) and 875 rpm with 2 g ball (E = 0.017 J); Figure S6: XRD patterns acquired during the syntheses at 550 rpm with 8 g ball and 875 rpm with 2 g ball.

Author Contributions: L.C. carried out the experimental activities and methodology, the syntheses by mechanochemical treatment, and the thermal, structural, and morphological analyses. L.C., with the other collaborators S.E., S.G., M.F. and G.M. analyzed the different data. In particular, S.E. and S.G. gave the main contribution to the phase investigation by crystallographic software. G.M. is the project administration and supervisor of L.C. with C.G. and L.S. M.F. and C.G. also wrote some part of original draft, review and edited the manuscript, and C.G. has contributed as funding acquisition. L.S. and R.B. have given the input for the work and have supported the literature search. All authors discussed the results, wrote their respective parts of the manuscript, and revised the overall manuscript. All authors have read and agreed to the published version of the manuscript.

Funding: This work and the activity of L.C. has been supported by a PhD program, MIUR special scholarship, within the joint agreement UNICA-UNISS for the PhD program in Chemical and Technological in Sciences. That PhD has been financed by PON-Ri scholarship (Programma Operativo Nazionale Ricerca e Innovazione 2014–2020, Fondo Sociale Europeo Regione Autonoma Sardegna). S.G., S.E., and G.M. acknowledge UNISS for the financial support received within the program "Fondo di Ateneo per la ricerca 2019".

Acknowledgments: The authors acknowledge the support of the CeSAR UNISS, Centro Servizi di Ateneo per la Ricerca of the University of Sassari, for making available several instrumental techniques to carry out materials characterization. Part of this work has been carried out in the framework of the ENABLES Project (http://www.enables-project.eu/), which received funding from the EU's Horizon 2020 research and innovation program under GA 730957.

Conflicts of Interest: The authors declare no conflict of interest.

References

1. Dunn, B.; Kamath, H.; Tarascon, J.-M. Electrical Energy Storage for the Grid: A Battery of Choices. *Science* **2011**, *334*, 928–935. [CrossRef]
2. Schipper, F.; Aurbach, D. A brief review: Past, present and future of lithium ion batteries. *Russ. J. Electrochem.* **2016**, *52*, 1095–1121. [CrossRef]
3. Islam, M.S.; Fisher, C.A.J. Lithium and sodium battery cathode materials: Computational insights into voltage, diffusion and nanostructural properties. *Chem. Soc. Rev.* **2014**, *43*, 185–204. [CrossRef]
4. Ding, Y.; Cano, Z.P.; Yu, A.; Lu, J.; Chen, Z. Automotive Li-Ion Batteries: Current Status and Future Perspectives. *Electrochem. Energy Rev.* **2019**, *2*, 1–28. [CrossRef]
5. Fares, R.L.; Webber, M.E. The impacts of storing solar energy in the home to reduce reliance on the utility. *Nat. Energy* **2017**, *2*, 17001. [CrossRef]
6. Heelan, J.; Gratz, E.; Zheng, Z.; Wang, Y.; Chen, M.; Apelian, D.; Wang, Y. Current and Prospective Li-Ion Battery Recycling and Recovery Processes. *JOM* **2016**, *68*, 2632–2638. [CrossRef]
7. Martin, G.; Rentsch, L.; Höck, M.; Bertau, M. Lithium market research—Global supply, future demand and price development. *Energy Storage Mater.* **2017**, *6*, 171–179. [CrossRef]
8. Canepa, P.; Gautam, G.S.; Hannah, D.C.; Malik, R.; Liu, M.; Gallagher, K.G.; Persson, K.A.; Ceder, G. Odyssey of Multivalent Cathode Materials: Open Questions and Future Challenges. *Chem. Rev.* **2017**, *117*, 4287–4341. [CrossRef] [PubMed]
9. Xie, J.; Zhang, Q. Recent Progress in Multivalent Metal (Mg, Zn, Ca, and Al) and Metal-Ion Rechargeable Batteries with Organic Materials as Promising Electrodes. *Small* **2019**, *15*, e1805061. [CrossRef]
10. Aurbach, D.; Lu, Z.; Schechter, A.; Gofer, Y.; Gizbar, H.; Turgeman, R.; Cohen, Y.; Moshkovich, M.; Levi, E. Prototype systems for rechargeable magnesium batteries. *Nature* **2000**, *407*, 724–727. [CrossRef]
11. Robba, A.; Vizintin, A.; Bitenc, J.; Mali, G.; Arčon, I.; Kavčič, M.; Žitnik, M.; Bučar, K.; Aquilanti, G.; Martineau-Corcos, C.; et al. Mechanistic Study of Magnesium–Sulfur Batteries. *Chem. Mater.* **2017**, *29*, 9555–9564. [CrossRef]
12. Ma, Z.; Macfarlane, D.R.; Kar, M. Mg Cathode Materials and Electrolytes for Rechargeable Mg Batteries: A Review. *Batter. Supercaps* **2019**, *2*, 115–127. [CrossRef]
13. Bertasi, F.; Hettige, C.; Sepehr, F.; Bogle, X.; Pagot, G.; Vezzù, K.; Negro, E.; Paddison, S.J.; Greenbaum, S.G.; Vittadello, M.; et al. A Key concept in Magnesium Secondary Battery Electrolytes. *ChemSusChem* **2015**, *8*, 3069–3076. [CrossRef] [PubMed]
14. Ponrouch, A.; Palacín, M.R. Post-Li batteries: Promises and challenges. *Philos. Trans. R. Soc. A Math. Phys. Eng. Sci.* **2019**, *377*, 20180297. [CrossRef] [PubMed]
15. Li, Z.; Han, L.; Wang, Y.; Li, X.; Lu, J.-L.; Hu, X. Microstructure Characteristics of Cathode Materials for Rechargeable Magnesium Batteries. *Small* **2019**, *15*, e1900105. [CrossRef]
16. Mohtadi, R.; Mizuno, F. Magnesium batteries: Current state of the art, issues and future perspectives. *Beilstein J. Nanotechnol.* **2014**, *5*, 1291–1311. [CrossRef]
17. Bodenez, V.; Dupont, L.; Laffont, L.; Armstrong, A.R.; Shaju, K.M.; Bruce, P.G.; Tarascon, J.-M. The reaction of lithium with CuCr2S4—Lithium intercalation and copper displacement/extrusion. *J. Mater. Chem.* **2007**, *17*, 3238. [CrossRef]
18. Liu, M.; Rong, Z.; Malik, R.; Canepa, P.; Jain, A.; Ceder, G.; Persson, K.A. Spinel compounds as multivalent battery cathodes: A systematic evaluation based on ab initio calculations. *Energy Environ. Sci.* **2015**, *8*, 964–974. [CrossRef]
19. Rong, Z.; Malik, R.; Canepa, P.; Gautam, G.S.; Liu, M.; Jain, A.; Persson, K.; Ceder, G. Materials Design Rules for Multivalent Ion Mobility in Intercalation Structures. *Chem. Mater.* **2015**, *27*, 6016–6021. [CrossRef]
20. Kim, C.; Phillips, P.J.; Key, B.; Yi, T.; Nordlund, D.; Yu, Y.-S.; Bayliss, R.D.; Han, S.-D.; He, M.; Zhang, Z.; et al. Direct Observation of Reversible Magnesium Ion Intercalation into a Spinel Oxide Host. *Adv. Mater.* **2015**, *27*, 3377–3384. [CrossRef]
21. Van Stapele, R. Chapter 8 Sulphospinels. In *Handbook of Ferromagnetic Materials*; North-Holland Publishing Company: Amsterdam, The Netherlands, 1982; Volume 3, pp. 603–745. [CrossRef]
22. Liu, M.; Jain, A.; Rong, Z.; Qu, X.; Canepa, P.; Malik, R.; Ceder, G.; Persson, K.A. Evaluation of sulfur spinel compounds for multivalent battery cathode applications. *Energy Environ. Sci.* **2016**, *9*, 3201–3209. [CrossRef]

23. Wustrow, A.; Key, B.; Phillips, P.J.; Sa, N.; Lipton, A.S.; Klie, R.F.; Vaughey, J.T.; Poeppelmeier, K.R. Synthesis and Characterization of MgCr2S4 Thiospinel as a Potential Magnesium Cathode. *Inorg. Chem.* **2018**, *57*, 8634–8638. [CrossRef] [PubMed]
24. Miura, A.; Ito, H.; Bartel, C.; Sun, W.; Rosero-Navarro, N.C.; Tadanaga, K.; Nakata, H.; Maeda, K.; Ceder, G. Selective metathesis synthesis of MgCr2S4 by control of thermodynamic driving forces. *Mater. Horiz.* **2020**, *7*, 1310–1316. [CrossRef]
25. Shaikh, M.; Iqbal, M.; Akhter, J.I.; Ahmad, M.; Zaman, Q.; Akhtar, M.; Moughal, M.; Ahmed, Z.; Farooque, M. Alloying of immiscible Ge with Al by ball milling. *Mater. Lett.* **2003**, *57*, 3681–3685. [CrossRef]
26. Delogu, F.; Cocco, G. Kinetics of structural evolution in immiscible Ag–Cu and Co–Cu systems under mechanical processing conditions. *Mater. Sci. Eng. A* **2005**, *402*, 208–214. [CrossRef]
27. Goo, N.; Hirscher, M. Synthesis of the nanocrystalline MgS and its interaction with hydrogen. *J. Alloys Compd.* **2005**, *404*, 503–506. [CrossRef]
28. Kyoi, D.; Rönnebro, E.; Kitamura, N.; Ueda, A.; Ito, M.; Katsuyama, S.; Sakai, T. The first magnesium– chromium hydride synthesized by the gigapascal high-pressure technique. *J. Alloys Compd.* **2003**, *361*, 252–256. [CrossRef]
29. Takacs, L. Self-sustaining reactions induced by ball milling. *Prog. Mater. Sci.* **2002**, *47*, 355–414. [CrossRef]
30. Baláž, P.; Baláž, M.; Achimovičová, M.; Bujňáková, Z.; Dutková, E. Chalcogenide mechanochemistry in materials science: Insight into synthesis and applications (a review). *J. Mater. Sci.* **2017**, *52*, 11851–11890. [CrossRef]
31. Liang, B.Y.; Wang, M.Z. Synthesis of Ti_3SiC_2 by mechanically induced self-sustaining reaction: Some mechanistic aspects. *Int. J. Self-Propagating High-Temp. Synth.* **2012**, *21*, 172–177. [CrossRef]
32. International Tables for Crystallography. *J. Appl. Crystallogr.* **1983**, *16*, 284. [CrossRef]
33. Lide, D.R. *Crc Handbook of Chemistry and Physics: A Ready-Reference Book of Chemical and Physical Data*; CRC Press: Boca Raton, FL, USA, 2004.
34. Wheast, R.C. Crc Standard thermodynamic properties of chemical substances. In *CRC Handbook of Chemistry and Physics*; CRC PRESS: Boca Raton, FL, USA, 2012; Volume 13, pp. 4–41. [CrossRef]
35. Waldner, P.; Sitte, W. Thermodynamic modeling of the Cr—S system. *Int. J. Mater. Res.* **2011**, *102*, 1216–1225. [CrossRef]
36. Abilov, C.; Kuliyev, A.; Hasanova, M. Phase Equilibra and Some Electrophycal Properties in the CuCr2S4—In System. *JMEST* **2015**, *2*, 267–270.
37. Delogu, F.; Mulas, G.; Schiffini, L.; Cocco, G. Mechanical work and conversion degree in mechanically induced processes. *Mater. Sci. Eng. A* **2004**, *382*, 280–287. [CrossRef]
38. Deidda, C.; Delogu, F.; Maglia, F.; Anselmi-Tamburini, U.; Cocco, G. Mechanical processing and self-sustaining high-temperature synthesis of TiC powders. *Mater. Sci. Eng. A* **2004**, 800–803. [CrossRef]
39. Takacs, L. Ball Milling-Induced Combustion in Powder Mixtures Containing Titanium, Zirconium, or Hafnium. *J. Solid State Chem.* **1996**, *125*, 75–84. [CrossRef]
40. Lutterotti, L. Total pattern fitting for the combined size-strain-stress-texture determination in thin film diffraction. *Nucl. Instrum. Methods Phys. Res. Sect. B Beam Interact. Mater. Atoms* **2010**, *268*, 334–340. [CrossRef]